

Zero Field Active Shielding.

Alain de Cheveigné(1, 2)

AUTHOR AFFILIATIONS:

(1) Laboratoire des Systèmes Perceptifs, UMR 8248, CNRS, France.

(2) Département d'Etudes Cognitives, Ecole Normale Supérieure, PSL, France.

CORRESPONDING AUTHOR:

Alain de Cheveigné, Audition, DEC, ENS, 29 rue d'Ulm, 75230, Paris, France,
Alain.de.Cheveigne@ens.fr, phone 00447912504027.

Abstract

Ambient field suppression is critical for accurate magnetic field measurements, and a requirement for certain low-field sensors to operate. The difference in magnitude between noise and signal (up to 10^9) makes the problem challenging, and solutions such as passive shielding, post-hoc processing, and most active shielding designs do not address it completely. Zero field active shielding (ZFS) achieves accurate field suppression with a feed-forward structure in which correction coils are fed by reference sensors via a matrix found using data-driven methods. Requirements are a sufficient number of correction coils and reference sensors to span the ambient field at the sensors, and to zero out the coil-to-reference sensor coupling. The solution assumes instantaneous propagation and mixing, but it can be extended to handle convolutional effects. Precise calculations based on sensor and coil geometries are not necessary, other than to improve efficiency and usability. The solution is simulated here but not implemented in hardware.

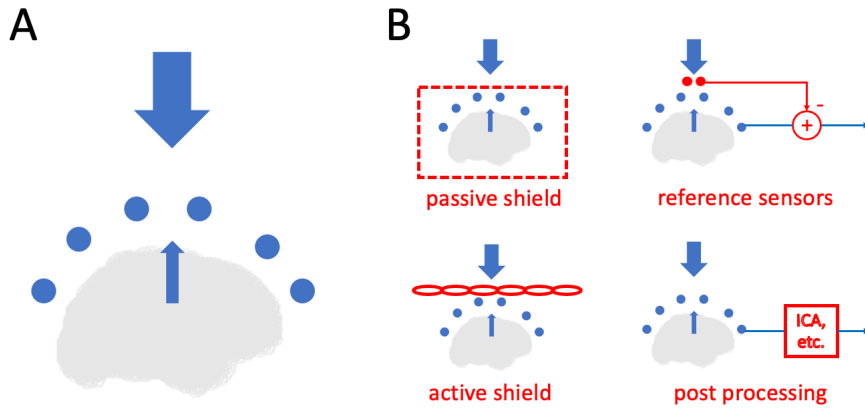


Figure 1: A: Magnetic fields from the brain are dwarfed by fields from ambient sources, including the earth’s magnetic field. B: Classic approaches to the problem: passive magnetic shielding, subtraction of signals from reference sensors, active magnetic shielding, downstream signal processing.

1 Introduction

Biomagnetic fields from the brain are much smaller than ambient magnetic noise fields from vehicles, machines or power lines, or the earth’s magnetic field (Fig. 1A). It is crucial to suppress those fields, but the task is daunting because of the levels involved: ambient fields may be larger than brain fields by a factor up to 10^9 (10^{18} in power), (Vrba, 2000). Large fields mask observations, and prevent certain devices such as optically-pumped magnetometers (OPM) from functioning. A strong DC field also makes magnetic measurements sensitive to structural vibration, as sensors move through that field.

The problem can be tackled by various means that are often used in combination (Fig. 1B) (Seymour et al., 2022). The most straightforward is *passive shielding*, with layers of mu-metal that mainly attenuate low frequency fields,

and aluminium or copper that attenuate high frequencies. Downsides are cost and weight, fixed location with limited space, a limited attenuation factor (10^2 to 10^4) (Vrba, 2000), and the need to de-gauss the shield in certain circumstances. Another common approach is to use *gradiometers* with a sensitivity that drops rapidly with distance, giving an advantage to brain sources (close to the sensors) over ambient sources (more distant).

A gradiometer is implemented by subtracting, from the field at the primary coil, the field at a secondary coil offset in space. The latter can be replaced by an array of *reference sensors*, shared across primary sensors, the output of which is scaled and subtracted from that of primary sensors in the digital domain. This allows flexibility to fine-tune the gradiometers, or to create synthetic gradiometers of higher order with enhanced rejection of ambient fields (Vrba, 2000). Appropriate coefficients can be found either analytically, based on the geometry, or by data-driven techniques such as regression (Vrba, 2000).

Yet another approach is *downstream processing* of the primary sensor data. Brain and ambient sources may be separated based on differences in the *spatial*, *spectral*, or *temporal* domains, using spatial filters, spectral filters, or blanking of time intervals with low SNR. Again, there is the choice between pre-determined solutions (e.g. Laplacian, re-referencing, or spherical harmonic decomposition in the spatial domain, or fixed filters in the spectral domain), and data-driven solutions (e.g. independent component analysis, ICA). A vast toolbox of linear data-driven methods is available for this purpose. If reference and primary sensor signals are treated uniformly as “data”, this approach subsumes the previous reference-based approach. A limitation of downstream processing is that it requires a wide dynamic range for sensors, analog-to-digital converters, and numerical representations. Superconducting quantum interference devices (SQUID) have a dynamic range better than 10^9 (Vrba, 2000), but that of OPMs is more

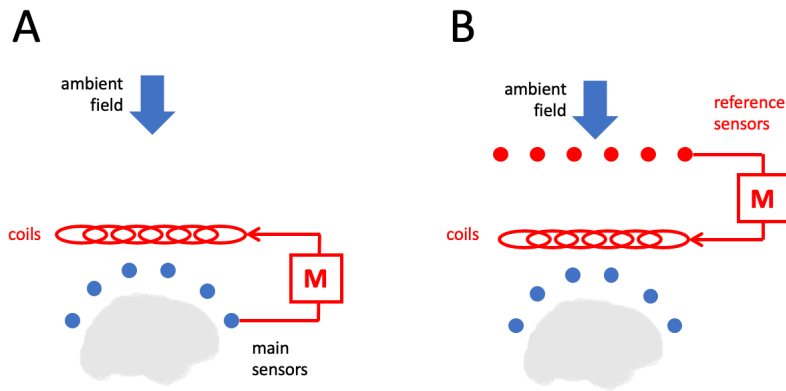


Figure 2: Two basic topologies of active shielding. A: Coils are driven from the main sensors via a matrix \mathbf{M} tuned to minimize the field at those sensors (feedback topology). B: Coils are driven from an array of reference sensors via a matrix \mathbf{M} tuned to minimize the field at the main sensors (feedback topology)

restricted.

A final approach is *active shielding* in which ambient fields are cancelled by correction coils of appropriate geometry, fed with a combination of fixed current (to cancel the earth’s field) and time-varying current (to cancel the fluctuating ambient field). An advantage is that fields are suppressed before transduction, which allows OPMs to function and reduces sensitivity to vibration for all types of sensor. The currents that feed the correction coils must track the time-varying ambient field, and for that the ambient field is sampled by an array of sensors, which drive the coils via a sensor-to-coil matrix \mathbf{M} . Two topologies are possible (Fig. 2). In the first, the drive comes from the *primary sensors* (or from reference sensors placed within the field of the coils) in a feedback topology (Fig. 2A). In the second, the drive comes from an array of dedicated *reference sensors*, ideally outside the field created by the coils, in a feedforward topology.

The feedback topology is a popular choice (Iivanainen et al., 2019; Pratt et al., 2021; Jazbinček et al., 2022; Hillebrand et al., 2023; Holmes et al., 2023; Władz-

iński et al., 2024), because it is simpler and avoids the need for reference sensors. Downsides are a risk of suppression of brain activity and instability of the corrective loop, the mitigation of which may reduce effectiveness. The feedforward topology does not have that issue, but it requires an array of reference sensors and is less common (e.g. Pyragius and Jensen, 2021).

The geometry of the coils must be such that the appropriate field pattern can be synthesized over the main sensors. Helmholtz coils are a popular choice, for example wired along the edges of the faces of a cube (Vrba, 2000; Sander et al., 2021), often in pairs to enhance the uniformity of the field. The coil geometry may be further enhanced for uniformity (Holmes et al., 2019), or larger numbers of coils may be used to achieve a specific non-uniform pattern using shimming techniques (Juchem et al., 2011; Kutschka et al., 2021; Holmes et al., 2022, 2023; Hobson et al., 2023). Their design requires accurate calculations and/or precision fabrication and/or calibration.

To summarize: suppression of ambient fields is crucial but challenging. Among approaches, downstream processing in the digital domain offers the greatest flexibility, but it requires a wide dynamic range and linearity that are hard to achieve with OPM sensors for which active shielding may be the most promising approach. Obstacles to be overcome include *instability* due to coupling between sensors and coils, *complexity* of the design, and *cost* in terms of hardware.

The method proposed in this paper aims to overcome the first two obstacles, possibly at the expense of aggravating the third. In a nutshell: stability is ensured by using a feedforward topology, together with a scheme to remove coil-sensor coupling, and complexity of design and calibration are addressed by data-driven algorithms. The feedforward solution is analogous to that employed by noise-cancelling headphones, in which an internal corrective sound field is driven from external microphones, with the objective of minimizing the sound field at an in-

ternal microphone.

The method is first described, then simulated with a simplified 2D “toy world” and with a more realistic 3D configuration using the Bio-Savart equation.

2 Methods

The method involves: (a) an array of reference sensors distinct from primary sensors, (b) an array of correction coils, (c) a reference sensor-to-coil transform matrix \mathbf{M} learned with a data-driven algorithm (Fig. 3A). The goal is to suppress the field at the primary sensors, but the method may be extended to suppress the ambient field within a volume, assuming smoothness in the region of the primary sensors.

2.1 Data model

Ambient source activity is represented by a matrix \mathbf{S} of size $T \times I$, primary sensor waveforms by \mathbf{X} of size $T \times J$, reference sensor waveforms by \mathbf{R} of size $T \times K$, and correction coil currents by \mathbf{Q} of size $T \times L$ (Fig. 3B), where I , J , K , L are the number of ambient sources, main sensors, reference sensors, and coils, respectively. Brain activity is ignored. The ambient magnetic field is a vector, but we can treat each component separately as a scalar. Its value, function of space and time, belongs to a vector space of very high dimensionality, but in practice we are interested in a smaller subspace spanned by the ambient field in the vicinity of the primary sensors. The dimensionality D of that space is at most I , number of ambient sources. It might be smaller if the number of main sensors is smaller ($J < I$), or if several sources produce fields with the same spatial pattern over sensors, or if several sources share the same time course.

To approximate and cancel the ambient field, the field space spanned by the

coils must include the field space spanned by the main sensors. This requires a number of coils L at least as large as D . Since coil currents are produced as a linear transform of reference sensor signals, the number K of reference sensors too must be at least D . To summarize, the method may require a number of coils and reference sensors potentially as large as the number I of ambient sources.

2.2 Finding \mathbf{M}

Referring to Fig. 3B, the ambient field \mathbf{S} is unknown, as are the source-to-sensor matrices \mathbf{A} and \mathbf{B} . The sensor signals \mathbf{X} and \mathbf{R} are observed, and the drive current \mathbf{Q} is also known. The coil-to-sensor matrices can be found by driving the coils with a current large enough to ignore the ambient field: $\mathbf{C} = \mathbf{Q}^\dagger \mathbf{X}$ and $\mathbf{D} = \mathbf{Q}^\dagger \mathbf{R}$, where \mathbf{Q}^\dagger is the pseudoinverse of the drive current \mathbf{Q} (Fig. 3C). It is also possible to estimate a reference-to-main sensor coupling matrix in response to the ambient field (in the absence of a coil current) as $\mathbf{P} = \mathbf{R}^\dagger \mathbf{X}$ (Fig. 3D).

Based on these elements, and *if the coil-to-reference sensor is small enough to be ignored*, the matrix \mathbf{M} can be calculated as

$$\mathbf{M} = -\mathbf{P}\mathbf{C}^\dagger. \quad (1)$$

The coil-to-reference coupling might be small if the reference sensors are distant from the coils or the correction coils are close to the primary sensors. However, if the coupling is not negligible, the corrective field leaks back to the reference sensors recursively (Fig. 3E, gray), and Eq. 1 does not ensure perfect field cancellation, and indeed the system might be unstable.

The problem can be addressed by using an augmented reference sensor array \mathbf{R}' and applying a matrix \mathbf{U} such that $\mathbf{R} = \mathbf{R}'\mathbf{U}$ is “shielded” from the coils, i.e. $\mathbf{D}\mathbf{U} = 0$ (Fig. 3F). For this to be possible, while still ensuring that \mathbf{R} spans the full ambient field, the augmented reference array must include at least $L + D$

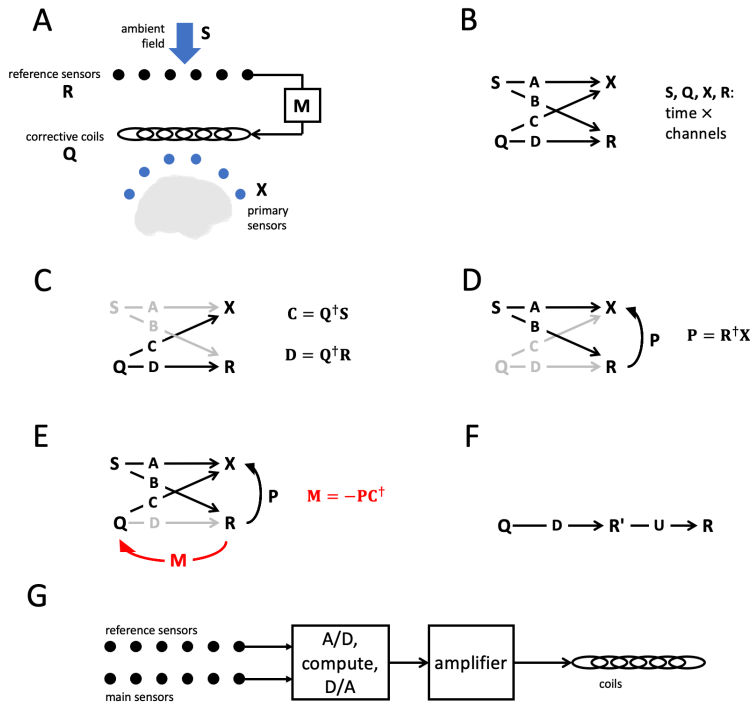


Figure 3: *A*: An array of correction coils is driven from an array of reference sensors via a feed-forward sensor-to-coil transform matrix M that is tuned to minimize the field at the primary sensors in the absence of brain activity. *B*: Block diagram of quantities and transforms. *C*: To estimate coil-to-sensor matrices C and D , coils are driven with a current Q large enough that the ambient field can be ignored. *D*: To estimate the reference-to-main sensor coupling matrix P , sensor outputs are observed in the absence of coil current. *E*: If the coil-to-reference matrix D is small enough be ignored, M can be estimated from C and P . *F*: If D is non-negligible, its effect can be removed by applying a "shielding" matrix U (see text). *G*: Structure of the required hardware.

sensors. Supposing that is the case, a convenient way to find the matrix \mathbf{U} is to drive the coils with a full-rank current matrix \mathbf{Q} , and apply principal component analysis (PCA) to the resulting matrix \mathbf{R}' . Since \mathbf{R}' is of rank at most L , the last D columns of the transform matrix map \mathbf{Q} to zero, which is the property that we need for \mathbf{U} . To summarize, the matrix \mathbf{M} is found in four steps:

1. A full-rank current matrix \mathbf{Q} is applied to the coils and matrix \mathbf{U} is derived by applying PCA to the reference array data matrix \mathbf{R}' .
2. Using the same current matrix \mathbf{Q} , the matrix \mathbf{C} is obtained as $\mathbf{C} = \mathbf{Q}^\dagger \mathbf{X}$.
3. In response to the ambient field (no current) the primary-to-reference coupling matrix is found as $\mathbf{P} = \mathbf{R}^\dagger \mathbf{X}$, where $\mathbf{R} = \mathbf{R}'\mathbf{U}$
4. \mathbf{M} is calculated as in Eq. 1.

The approach is attractive because, *if its requirements are fulfilled*, the solution ensures perfect cancellation at the primary sensors. As it is data-driven, there is no need for precise calculations based on coil or sensor geometry. The hardware structure is schematized in Fig. 3 G and requirements are discussed in more detail in the Discussion.

3 Results

The method is first simulated within a simplified 2D “toy world” that allows easy visualization. It is then simulated in a more complex 3D configuration using Biot-Savart equations. These set the stage for a hardware implementation which remains for a future study.

3.1 A toy world

To gain insight, a “toy world” is defined in which sensor and sources are located within a plane, and each source produces a field that varies with distance as $1/d^2$. This captures the main features of the problem while allowing for easy visualization: complexities related to 3D positions and orientation of sources and sensors are conveniently ignored.

Sources and sensors are located within a square as shown in Fig. 4B (8 ambient sources as circles, 8 main sensors as crosses) and Fig. 4C (12 coils as red circles, 24 reference sensors as red crosses). Based on these positions, the source-to-sensor gain matrices \mathbf{A}_0 , \mathbf{B}_0 , \mathbf{C}_0 and \mathbf{D}_0 are calculated using the $1/d^2$ law, the subscript indicating ground truth. These are used to simulate the “physics” of the system but are not observable and are not used to obtain \mathbf{M} .

In a first step, the coils were driven with a 1000×12 matrix \mathbf{Q} of Gaussian random numbers and the reference sensor data matrix was obtained as $\mathbf{R}' = \mathbf{Q}\mathbf{D}_0$. PCA was applied to \mathbf{R}' , and the 24×12 shielding matrix \mathbf{U} was set to the last 12 columns of the 24×24 PCA matrix. In a second step, using that same driving matrix, the main sensor data matrix was calculated as $\mathbf{X} = \mathbf{Q}\mathbf{C}_0$, and the coil-to-main gain matrix was estimated as $\mathbf{C} = \mathbf{Q}^\dagger \mathbf{X}$ (\mathbf{C} is of course equal to the ground truth \mathbf{C}_0). In a third step, a 1000×8 matrix \mathbf{S} of Gaussian-distributed random numbers was used to simulate ambient source activity, and sensor data matrices were calculated as $\mathbf{X} = \mathbf{S}\mathbf{A}_0$ and $\mathbf{R}' = \mathbf{S}\mathbf{B}_0$. The shielding matrix was applied to obtain $\mathbf{R} = \mathbf{R}'\mathbf{U}$, and the reference-to-main coupling matrix was calculated as $\mathbf{P} = \mathbf{X}^\dagger \mathbf{R}$. In a fourth and final step, the reference-to-coil driving matrix was calculated as $\mathbf{M} = -\mathbf{P}\mathbf{C}^\dagger$.

The simulation is illustrated in Fig. 4. If a single ambient source is active, the amplitude of its field (color) decreases as $1/d^2$ (Fig. 4A). If all sources are active with uncorrelated equal amplitude waveforms, the RMS ambient field (color) is

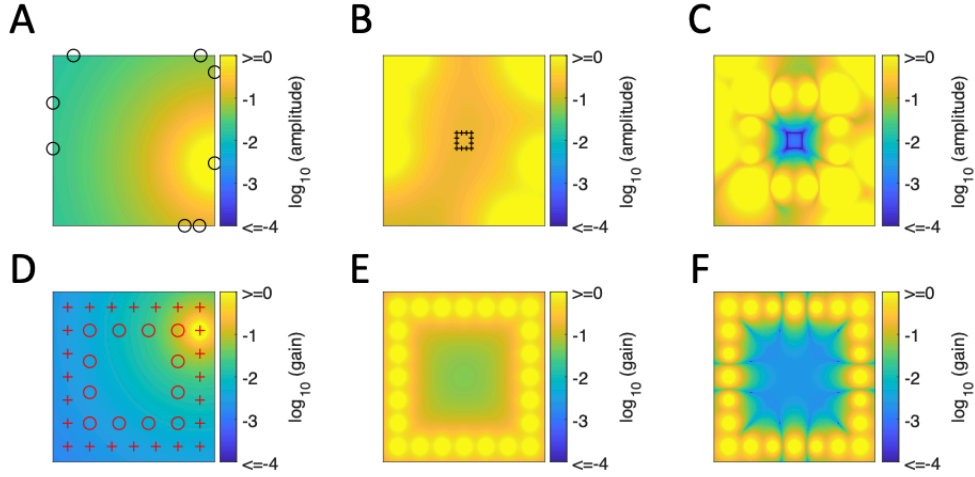


Figure 4: Toy world simulation. A: Ambient sources (circles) are located on the edges of a square. The amplitude of the field (color) varies with distance from a source as $1/d^2$ (here one source is active). B: Same as A, but all eight sources are active (same amplitude, uncorrelated waveforms, color represents the RMS amplitude averaged over sources). Crosses show the positions of the main sensors. C: Residual RMS amplitude of the ambient field after correction. The field at the positions of the main sensors is reduced by a factor larger than 10^5 (blue, compare with B). D-F: cancellation of the coil-to-reference sensor coupling. D: Reference sensors are represented as red crosses, coils as red circles. Color: gain as a function of position for one reference sensor. E: RMS gain as a function of position averaged over all reference sensors. The RMS gain is non-zero at the position of the coils, implying that **D** is not negligible. F: Applying the shielding matrix **U** modifies the gain map so that RMS gain is now zero at the coils. Note the fine blue dots.

non-zero at the main sensors (crosses in Fig. 4B). With active shielding, the field at the sensors is reduced by a factor greater than 10^5 (Fig. 4C).

A critical step is cancellation of the coil-to-reference sensor coupling. Figure 4D shows the location-to-sensor gain map for one reference sensor, and Fig. 4E shows the RMS location-to-sensor gain averaged over reference sensors. This gain is non-zero at the positions of the coils, implying that \mathbf{D} is not negligible. However, applying the “shielding” matrix \mathbf{U} changes this gain map as shown in Fig. 4F. The RMS gain is now zero at the positions of the coils (blue points), but non-zero at the ambient sources, implying that \mathbf{R} is invariant with respect to the coils, yet tracks the ambient sources.

The method is effective within this simplified toy world (compare Fig. 4B and C). The next simulation extends the result to a more realistic situation involving sensors and sources distributed in 3D space, with fields varying according to the Biot-Savart law.

3.2 Simulation based on the Biot-Savart law

A set of 274 main sensors (magnetometers) was distributed with positions and orientations corresponding to the base coils of gradiometers in a CTF magnetoencephalograph. A set of 54 simulated ambient sources was distributed on a cube of side 4 m centered on the CTF coordinate origin (Fig. 5A), a set of 54 “coils” (modeled as dipolar sources) was distributed on a cube of side 1 m, and a set of 108 reference sensors was distributed on two cubes of side 3 m and 3.3 m, all centered on the CTF coordinate origin (Fig. 5A). Ambient sources, reference sensors, and coils had random orientations. Source-to-sensor gain matrices \mathbf{A}_0 , \mathbf{B}_0 , \mathbf{C}_0 and \mathbf{D}_0 were calculated according to the Biot-Savart equation using code from the VBMEG toolbox (vbmeg.atr.jp) (Takeda et al., 2019).

The active shielding matrix \mathbf{M} was calculated following the same procedure

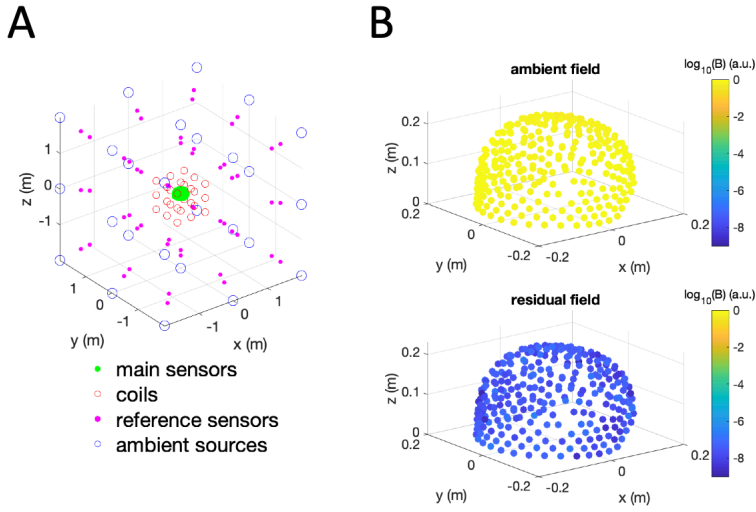


Figure 5: Simulation based on the Biot-Savart law. A: locations of main sensors (green dots), coils (red circles), reference sensors (magenta dots), and ambient sources (black circles). Coils, reference sensors and ambient sources have random orientations, main sensors are oriented as in a CTF MEG system. B: RMS magnitude of ambient field over main sensors (arbitrary units). C: same, after ambient field suppression.

as in the previous simulation. If all ambient sources were active, with uncorrelated waveforms and equal amplitudes, the ambient field RMS amplitude at the sensors would appear as in Fig. 5B (top, arbitrary units). With active shielding, the residual field RMS amplitude is reduced as shown in Fig. 5B (bottom). Relative to the ambient field, the attenuation factor is better than 10^8 .

This simulation suggests that the method might be effective in a real-world situation. A caveat is that simulated ambient sources were modelled as magnetic dipoles, whereas real ambient sources might be more complex. Coils too were simulated as dipoles, in contrast to e.g. Helmholtz coils or more complex geometries. However, there is nothing to suggest that the method, which depends on algebraic properties, would not extend to those geometries.

4 Discussion

Zero field active shielding (ZFS) aims to perfectly cancel the ambient field at the primary sensors (hence its name). The cost in sensors, coils and associated electronics is potentially larger than in other schemes, but perhaps not out of proportion with the cost of sophisticated sensor technology. It may be justified by the final quality of the data, and the enabling effects on the technology.

4.1 Requirements

1. Coil array. The magnetic field produced by the coils must reproduce (so as to cancel it) the ambient field spatial pattern across the J primary sensors. As argued earlier, this might require up to $L = J$ coils, although a smaller number might suffice if the ambient sources are fewer than J , or if they are sufficiently distant so that their field can be approximated by a smaller number of spatial components (Tierney et al., 2021), or if their time-course is shared with other sources so the spatial patterns can be merged. Three orthogonal coils are required to create a vector field at a point, nine additional coils allow to control first-order gradients, and 32 more allow to control second-order gradients, and so on. The geometry is not critical as long as coils are placed such that their field patterns are not redundant. Specific geometries might be optimized to enhance field uniformity or reduce current requirements.

2. Reference sensor array. The reference sensor array must span the *signal space* carried by the ambient field at the primary sensors. Each signal component is associated with a spatial component, and so the reference sensors must fully sample the *field space* of the ambient sources, at least the part that impinges on the primary sensors. For this, up to $K = J$ reference sensors might be required,

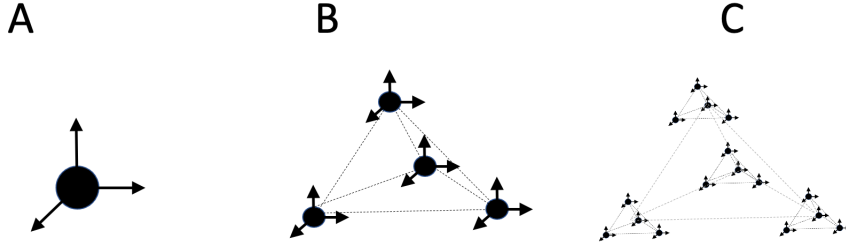


Figure 6: Sampling the spatially complex ambient field. A: The three components of the field require three sensors. B: First-order gradients require 9 additional sensors. C: Second-order gradients require additional 36 sensors (total: 48). The geometry can be adjusted based on known properties of the ambient field, or architectural constraints, but degenerate configurations (e.g. 4 or more similarly-oriented sensors in a plane) should be avoided.

although a smaller number might suffice if the ambient field is simple (Tierney et al., 2021). Fig. 6 illustrates geometries that captures the field and its first two gradients, however other geometries are acceptable as long as no two sensors are redundant (e.g. four or more similarly-oriented sensors in a plane, etc.).

3. Coil-to-reference sensor coupling. Equation 1 holds only if the coil-to-reference sensor is negligible, and indeed the system might become unstable otherwise. Coupling could be reduced by placing coils within each device, e.g. (Fourcault et al., 2021; Tayler et al., 2022; Badier et al., 2023), or placing the reference sensors close to the ambient sources, or outside a shielded room. A more widely applicable solution is to augment the number of reference sensors by L and derive a coupling-suppressing matrix \mathbf{U} as described in the Methods. As an alternative to augmenting the reference array, one could instead augment the coil array and drive it via a $L \times (L + D)$ matrix \mathbf{V} such that $\mathbf{VD} = 0$, again nulling the coil-to-sensor coupling. Which option is chosen depends on relative costs and other constraints.

4. Other requirements and issues. The coefficients of \mathbf{M} are not constrained in magnitude, and thus the data-driven solution might entail impracticably large values of *current*. A solution may be to increase L so as to allow a wider space of solutions, and introduce an additional constraint in the calculation of \mathbf{M} to favour those with lower peak currents. *Current noise* is also potentially an issue because it directly translates into magnetic noise at the primary sensors (Durdaut et al., 2021). Low-noise current sources are required, or the noise must be measured and suppressed downstream (see below).

Latency affects responsiveness to transients and thus reduces the bandwidth of the correction mechanism. Latency associated with digital conversion and processing might be avoided if \mathbf{M} is implemented as a programmable analog gain matrix (e.g. Schlottmann and Hasler, 2011). *Convolutional* effects may arise, for example due to dispersive properties of shielding materials. To address them, observations \mathbf{X} and \mathbf{Y} may be augmented with time shifts (de Cheveigné and Simon, 2007) to allow the data-driven solution to implement an FIR filter. Convolutional kernels other than shifts are also possible. Estimation of \mathbf{C} and \mathbf{P} requires properly-functioning primary sensors, which might not be the case for OPMs if the ambient field is too large. To handle that situation, the primary sensor array may need to be augmented with high-field sensors so as to *bootstrap* the system.

An important consideration is that the main-to-reference sensor matrix \mathbf{P} is *data-driven*, learned during a calibration phase in the absence of brain activity. Two potential issues are (a) non-stationarity, for example an important ambient source might not be active during the calibration phase, and (b) the predominantly low-pass characteristic of ambient fields, that reduces effective degrees of freedom, and thus increases the risk of overfitting. Adaptive recalibration is an option, possibly involving out-of-band calibration signals to avoid interference with brain signals.

Objects with particular magnetic properties (e.g. hysteresis) might invalidate the assumptions of linearity and time-invariance. This situation may be handled by assuming an additional ambient source at the location of that object. Likewise, a moving vehicle or machine, which does not have a well-defined “spatial position” may be handled by assuming multiple sources located along the trajectory. Whether these solutions are satisfactory is a question to be answered empirically.

4.2 Relation with other approaches

ZFS might conceivably obviate the need for *passive shielding*. If so, it would bring down cost and bring MEG closer to functioning in the clinic or in the street.

The main contender to ZFS is the feedback topology of (Fig. 2A). Most schemes follow that design which avoids the cost of reference sensors, is simpler, and can be implemented locally as in within-device active shielding. The feedforward topology (Fig. 2B) has also been proposed in the past (e.g. Pyragius and Jensen, 2021) but it is less common. Are the two approaches equivalent or interchangeable? It is simple to see that the answer is no. If the input of the current-control plant (\mathbf{M} in Fig. 2A) is zero, its output cannot be a time-varying current as required to cancel a time-varying ambient field. As another argument, the feedback loop cannot distinguish between brain and ambient field, other than by spectral content or, in the case of a sensor array, spatial content as exploited for example by a decomposition in spherical harmonics (Tierney et al., 2022; Mellor et al., 2022; Tierney et al., 2024). The feedback topology allows an *approximate* solution, but it may have a limited frequency response and be at risk of instability. The feedforward topology avoids those issues.

ZFS uses whatever coil geometry is available, in contrast to schemes that require carefully-designed coils to maximize field uniformity (Holmes et al., 2018, 2019, 2023; Kutschka et al., 2021), or multiple coils to achieve a specific non-

uniform pattern using shimming techniques (Juchem et al., 2011; Kutschka et al., 2021; Holmes et al., 2022, 2023; Hobson et al., 2023). ZFS sidesteps the need for precise coil design, fabrication, or calibration by using data-driven techniques, but it is clear that it can benefit from a coil geometry optimized to best approximate the ambient field with minimum current. Many previous schemes assume a rather small number of coils (but see Holmes et al 2023) and/or reference sensors, presumably for simplicity and to limit cost. Here, this was *not* a design goal (Sect. 2), but in practice smaller numbers may be forced by cost constraints, in which case performance is expected to degrade gracefully.

Another major contender for ZFS is *downstream processing* in the digital domain, from which ZFS's data-driven methods are borrowed. Indeed, if the reference sensors signals were available to downstream processing, subtraction of the ambient field could occur at that stage in addition to the many other operations possible in the digital domain. The primary reason to perform the subtraction in the field domain is to allow the use of sensors with a limited dynamic range, although an added benefit is reduced artifact from motion in a non-zero magnetic field, for example due to structural vibration.

It is important to point out that ZFS is not exclusive of other schemes, with which it could be associated to form a hybrid solution. As an example, ZFS could avail itself of on-device coils to deliver the shielding locally at each device (Fig. 7A). Alternatively, known imperfections of ZFS (e.g. latency, or clipping, or current noise) could be fed a to downstream processing module so they can be factored out (Fig. 7B). Or the entire system (coils and main and reference sensors) could be surrounded by Helmholtz coils driven in a simple feed-back loop for the purpose of reducing the DC field to allow the main ZFS system to be implemented with lower-field sensors.

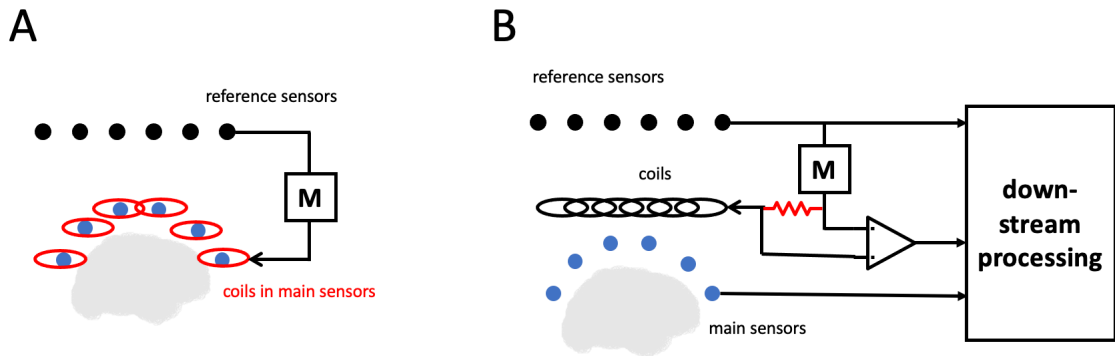


Figure 7: Hybrid schemes. A: Coils are within sensors. B: The current within each coil is measured and made available to downstream processing, to factor out current noise and/or errors due to latency.

4.3 Widening the application space

MEG is on the cusp of paradigm shift, going from expensive lab-based systems with heavy shielding and cryogenics, to cheaper and more flexible systems using OPMs. Moving “from the lab to the street” (or at least to the clinic) would considerably widen the application space. However, while OPMs are cheaper and more flexible than SQUIDs, they are if anything *more* prone to the effects of ambient fields (Seymour et al., 2022). This puts active shielding center stage.

Ideally, we would like to record from a freely-moving subject within a large space. One option is to enclose the space with an array of coils and use ZFS to minimize the field across the space, using a dedicated array of “main sensors” to sample the space densely. Alternatively, the space might be sampled dynamically (e.g. Rawlik, 2018; Rea et al., 2021). For that purpose, the geometry of the coil array may be optimized for field uniformity (e.g. Holmes et al., 2018, 2019, 2023). . A second option, still using an array of coils enclosing the space, is to track the location of the subject and use that information to steer a location-dependent solution (possibly pre-trained based on sampling) to null the field at that location

(e.g. Rea et al., 2021; Holmes et al., 2023). A third option is to use an array of coils that move with the subject, possibly within the sensors, again using a position-dependent solution. The purpose of this enumeration is not to review these approaches, but rather to point out that the forward topology of ZFS might make them easier to design.

In addition to MEG, magnetocardiography (MCG), peripheral nerve or spinal cord measurements, or other industrial or scientific applications, might all benefit from progress in active shielding.

Conclusion

Ambient field suppression is important for accurate magnetic field measurements, in particular to allow low-field sensors to operate. Several design choices are critical for an accurate solution: a feed-forward topology, a sufficient number of coils and reference sensors, and precautions to avoid coil-to-sensor coupling. On that basis, and assuming linear, time invariant, and instantaneous propagation and processing, the ambient field can be accurately canceled at the main sensors or over a wider space assuming smoothness of the fields. The method performed well in simulations, setting the stage for a future implementation in hardware.

Acknowledgements

This work was supported by grants ANR-10-LABX-0087 IEC, ANR-10-IDEX-0001-02 PSL, and ANR-17-EURE-0017. The paper benefitted from useful comments from Jacob Reichel, Tilmann Sander-Thoemmes, Gen Uehara, and members of the UCL OPM group.

References

References

- Badier JM, Schwartz D, Bénar CG, Kanzari K, Daligault S, Romain R, Mityukovskiy S, Fourcault W, Josselin V, Le Prado M, Jung J, Palacios-Laloy A, Romain C, Bartolomei F, Labyt E, Bonini F (2023) Helium Optically Pumped Magnetometers Can Detect Epileptic Abnormalities as Well as SQUIDs as Shown by Intracerebral Recordings. *eneuro* 10:ENEURO.0222–23.2023.
- de Cheveigné A, Simon JZ (2007) Denoising based on time-shift PCA. *Journal of Neuroscience Methods* 165:297–305.
- Durdaut P, Wolframm H, Höft M (2021) Low-Frequency Magnetic Noise in Statically-Driven Solenoid for Biasing Magnetic Field Sensors arXiv:2006.08515 [physics].
- Fourcault W, Romain R, Le Gal G, Bertrand F, Josselin V, Le Prado M, Labyt E, Palacios-Laloy A (2021) Helium-4 magnetometers for room-temperature biomedical imaging: toward collective operation and photon-noise limited sensitivity. *Optics Express* 29:14467.
- Hillebrand A, Holmes N, Sijsma N, O’Neill GC, Tierney TM, Liberton N, Stam AH, Van Klink N, Stam CJ, Bowtell R, Brookes MJ, Barnes GR (2023) Non-invasive measurements of ictal and interictal epileptiform activity using optically pumped magnetometers. *Scientific Reports* 13:4623.
- Hobson PJ, Holmes N, Patel P, Styles B, Chalmers J, Morley C, Davis A, Packer M, Smith TX, Raudonyte S, Holmes D, Harrison R, Woolger D, Sims D, Brookes MJ, Bowtell R, Fromhold M (2023) Benchtop Magnetic Shielding for

- Benchmarking Atomic Magnetometers. *IEEE Transactions on Instrumentation and Measurement* 72:1–9.
- Holmes N, Leggett J, Boto E, Roberts G, Hill RM, Tierney TM, Shah V, Barnes GR, Brookes MJ, Bowtell R (2018) A bi-planar coil system for nulling background magnetic fields in scalp mounted magnetoencephalography. *NeuroImage* 181:760–774.
- Holmes N, Rea M, Chalmers J, Leggett J, Edwards LJ, Nell P, Pink S, Patel P, Wood J, Murby N, Woolger D, Dawson E, Mariani C, Tierney TM, Mellor S, O’Neill GC, Boto E, Hill RM, Shah V, Osborne J, Pardington R, Fierlinger P, Barnes GR, Glover P, Brookes MJ, Bowtell R (2022) A lightweight magnetically shielded room with active shielding. *Scientific Reports* 12:13561.
- Holmes N, Rea M, Hill RM, Leggett J, Edwards LJ, Hobson PJ, Boto E, Tierney TM, Rier L, Rivero GR, Shah V, Osborne J, Fromhold TM, Glover P, Brookes MJ, Bowtell R (2023) Enabling ambulatory movement in wearable magnetoencephalography with matrix coil active magnetic shielding. *NeuroImage* 274:120157.
- Holmes N, Tierney TM, Leggett J, Boto E, Mellor S, Roberts G, Hill RM, Shah V, Barnes GR, Brookes MJ, Bowtell R (2019) Balanced, bi-planar magnetic field and field gradient coils for field compensation in wearable magnetoencephalography. *Scientific Reports* 9:14196.
- Iivanainen J, Zetter R, Grön M, Hakkarainen K, Parkkonen L (2019) On-scalp MEG system utilizing an actively shielded array of optically-pumped magnetometers. *NeuroImage* 194:244–258.
- Jazbinček V, Marhl U, Sander T (2022) SERF-OPM Usability for MEG in Two-Layer-Shielded Rooms In Labyt E, Sander T, Wakai R, editors, *Flexible High*

- Performance Magnetic Field Sensors*, pp. 179–193. Springer International Publishing, Cham.
- Juchem C, Brown PB, Nixon TW, McIntyre S, Rothman DL, De Graaf RA (2011) Multicoil shimming of the mouse brain. *Magnetic Resonance in Medicine* 66:893–900.
- Kutschka H, Doeller CF, Haueisen J, Maess B (2021) Magnetic field compensation coil design for magnetoencephalography. *Scientific Reports* 11:22650.
- Mellor S, Tierney TM, O’Neill GC, Alexander N, Seymour RA, Holmes N, López JD, Hill RM, Boto E, Rea M, Roberts G, Leggett J, Bowtell R, Brookes MJ, Maguire EA, Walker MC, Barnes GR (2022) Magnetic field mapping and correction for moving op-meg. *IEEE Transactions on Biomedical Engineering* 69:528–536.
- Pratt EJ, Ledbetter M, Jiménez-Martínez R, Shapiro B, Solon A, Iwata GZ, Garber S, Gormley J, Decker D, Delgadillo D, Dellis AT, Phillips J, Sundar G, Leung J, Coyne J, McKinley M, Lopez G, Homan S, Marsh L, Zhang M, Maurice V, Siepser B, Giovannoli T, Leverett B, Lerner G, Seidman S, DeLuna V, Wright-Freeman K, Kates-Harbeck J, Lasser T, Mohseni H, Sharp T, Zorzos A, Lara AH, Kouhzadi A, Ojeda A, Chopra P, Bednarke Z, Henninger M, Alford JK (2021) Kernel Flux: a whole-head 432-magnetometer optically-pumped magnetoencephalography (OP-MEG) system for brain activity imaging during natural human experiences In Shahriar SM, Scheuer J, editors, *Optical and Quantum Sensing and Precision Metrology*, p. 101, Online Only, United States. SPIE.
- Pyragius T, Jensen K (2021) A high performance active noise control system for magnetic fields. *Review of Scientific Instruments* 92:124702.

- Rawlik M (2018) Active Magnetic Shielding and Axion-Dark-Matter Search Ph.D. diss., ETH Zurich.
- Rea M, Holmes N, Hill RM, Boto E, Leggett J, Edwards LJ, Woolger D, Dawson E, Shah V, Osborne J, Bowtell R, Brookes MJ (2021) Precision magnetic field modelling and control for wearable magnetoencephalography. *NeuroImage* 241:118401.
- Sander TH, Marhl U, Brühl R, Middelman T, Jazbi V (2021) A 50 channel optically pumped magnetometer MEG in an externally actively shielded two-layer room. *International Journal of Biomagnetism* 23:5/1–5.
- Schlottmann CR, Hasler PE (2011) A Highly Dense, Low Power, Programmable Analog Vector-Matrix Multiplier: The FPAA Implementation. *IEEE Journal on Emerging and Selected Topics in Circuits and Systems* 1:403–411.
- Seymour RA, Alexander N, Mellor S, O’Neill GC, Tierney TM, Barnes GR, Maguire EA (2022) Interference suppression techniques for OPM-based MEG: Opportunities and challenges. *NeuroImage* 247:118834.
- Takeda Y, Suzuki K, Kawato M, Yamashita O (2019) MEG Source Imaging and Group Analysis Using VBMEG. *Frontiers in Neuroscience* 13:241.
- Taylor MCD, Mouloudakis K, Zetter R, Hunter D, Lucivero VG, Bodenstedt S, Parkkonen L, Mitchell MW (2022) Miniature biplanar coils for alkali-metal-vapor magnetometry. *Physical Review Applied* 18:014036 arXiv:2204.01370 [physics].
- Tierney TM, Alexander N, Mellor S, Holmes N, Seymour R, O’Neill GC, Maguire EA, Barnes GR (2021) Modelling optically pumped magnetometer interference in MEG as a spatially homogeneous magnetic field. *NeuroImage* 244:118484.

- Tierney TM, Mellor S, O'Neill GC, Timms RC, Barnes GR (2022) Spherical harmonic based noise rejection and neuronal sampling with multi-axis OPMs. *NeuroImage* 258:119338.
- Tierney TM, Seedat Z, St Pier K, Mellor S, Barnes GR (2024) Adaptive multipole models of optically pumped magnetometer data. *Human Brain Mapping* 45:e26596.
- Vrba J (2000) Multichannel SQUID Biomagnetic Systems In Weinstock H, editor, *Applications of Superconductivity*, pp. 61–138. Springer Netherlands, Dordrecht.
- Władziński M, Jodko-Władzińska A, Sander TH (2024) Active Compensation for OPM-MEG Inside a Two-Layer Magnetically Shielded Room In Jarm T, Šmerc R, Mahnič-Kalamiza S, editors, *9th European Medical and Biological Engineering Conference*, Vol. 112, pp. 48–54. Springer Nature Switzerland, Cham
Series Title: IFMBE Proceedings.